Ultramicroscopy 246 (2023) 113673

Contents lists available at ScienceDirect

Ultramicroscopy

journal homepage: www.elsevier.com/locate/ultramic

Decomposition of CrN induced by laser-assisted atom probe tomography

Helene Waldl [a,*], Marcus Hans [b], Maximilian Schiester [c], Daniel Primetzhofer [d], Michael Burtscher [e], Nina Schalk [a], Michael Tkadletz [c]

[a] Christian Doppler Laboratory for Advanced Coated Cutting Tools, Montanuniversität Leoben, Franz Josef-Straße 18, 8700 Leoben, Austria
[b] Materials Chemistry, RWTH Aachen University, Kopernikusstraße 10, 52074 Aachen, Germany
[c] Department of Materials Science, Montanuniversität Leoben, Franz Josef-Straße 18, 8700 Leoben, Austria
[d] Department of Physics and Astronomy, Uppsala University, Box 516, 75120 Uppsala, Sweden
[e] Department of Materials Science, Chair of Materials Physics, Montanuniversität Leoben, 8700 Leoben, Austria

ARTICLE INFO

Keywords:
Atom probe tomography
Laser pulse energy
CrN
CrAlN
Elemental composition

ABSTRACT

It is known that measurement parameters can significantly influence the elemental composition determined by atom probe tomography (APT). Especially results obtained by laser-assisted APT show a strong effect of the laser pulse energy on the apparent elemental composition. Within this study laser-assisted APT experiments were performed on $Cr_{0.51}N_{0.49}$ and thermally more stable $(Cr_{0.47}Al_{0.53})_{0.49}N_{0.51}$, comparing two different base temperatures (i.e. 15 and 60 K), laser wavelengths (i.e. 532 and 355 nm) and systematically modified laser pulse energies. Absolute chemical compositions from laser-assisted APT were compared to data obtained from ion beam analysis. The deduced elemental composition of CrN exhibited a strong increase of the Cr content when the laser pulse energy was increased for both laser wavelengths. For low laser pulse energies Cr, CrN, N and N_2 ions were identified, while the amount of detected Cr ions increased and the amount of N ions strongly decreased at higher laser pulse energies. Further, increased detection of more complex Cr-containing ions such as Cr_2N at the expense of CrN was observed at higher pulse energies. At the highest pulse energy levels used within this work, the resulting Cr content was > 80 at%, dominated by the amount of detected elemental Cr ions. The change of the mass spectrum of the detected ions with increasing laser pulse energy provides evidence that high laser pulse energies initiate the decomposition of CrN during the APT measurement, consistent with the known thermal decomposition path into Cr_2N and subsequently into Cr and gaseous N. In contrast, variation of the laser pulse energy for the thermally more stable CrAlN resulted only in a slight increase of Cr and a decrease of the resulting concentrations of Al and N with increasing laser pulse energy and no change in the type of detected ions. In conclusion, within the present study, the decomposition of a coating material with low thermal stability induced by laser-assisted APT was reported for the first time, emphasizing the importance of the selection of suitable measurement parameters for metastable materials, which are prone to thermal decomposition.

1. Introduction

Nowadays high-performance materials are indispensable for our daily life. Since these materials are often nano-structured, the application of high-resolution methods is essential to gain detailed knowledge about their microstructure and properties, facilitating the development of new or the further development of already established materials systems. In order to tailor the properties, information of the exact elemental composition, not only on a global scale but also locally, is of major importance. However, commonly used methods suffer from limited lateral and depth resolution [1,2]. These limitations can be overcome by atom probe tomography (APT), which allows the determination of the three-dimensional elemental composition close to the atomic scale [3]. The basic principle of APT measurements of conductive materials is the evaporation and ionization of single atoms from a needle-like specimen by applying high voltage pulses [3,4]. The ions are accelerated towards a position-sensitive detector with integrated time-of-flight mass spectrometry to determine the position and species of the evaporated atoms [4]. For less- or even non-conductive materials, laser pulses are applied to thermally activate the evaporation of the atoms [4,5]. While the development of thermally-assisted field-evaporation via laser-pulsing is more recent, for many materials its influence

* Corresponding author.
E-mail address: helene.waldl@unileoben.ac.at (H. Waldl).

https://doi.org/10.1016/j.ultramic.2022.113673
Received 18 October 2022; Received in revised form 22 December 2022; Accepted 26 December 2022
Available online 27 December 2022

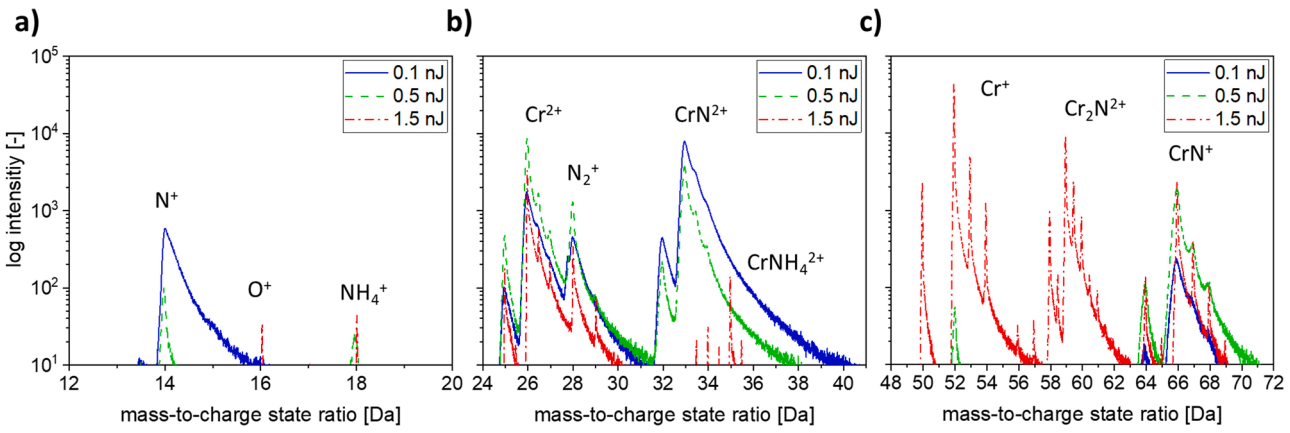

Fig. 1. Mass spectra for CrN measured with different laser pulse energies (green laser) in the range of a) 12-20 Da, b) 24-41 Da and c) 48-72 Da.

on measurement results is not completely understood [6]. Especially the elemental composition for nitride and oxide based materials can be significantly affected by the measurement parameters, in particular by the laser pulse energy, which has already been shown in literature [2, 6–8]. For a close-to-stoichiometric TiAlN coating it has been demonstrated that an increasing laser pulse energy considerably decreases the amount of detected N [2,9]. Thus, detailed studies of the influence of different process parameters on the deduced concentration maps are crucial before measuring new materials to evaluate the measurement accuracy.

CrN is a metastable transition metal nitride, that can be synthesized by physical vapor deposition and is commonly applied as a coating [10]. At temperatures between 450 and 900°C CrN starts to thermally decompose [11–13]. First, gaseous N is released and causes formation of Cr_2N, which subsequently further decomposes into Cr and gaseous N [12]. With the addition of Al to CrN, a thermally more stable solid solution is formed [10,14]. Upon annealing of CrAlN, first AlN precipitates are formed and thus the matrix gets enriched in Cr [14]. This matrix subsequently decomposes via Cr_2N into Cr and gaseous N following the same decomposition route as CrN, however at much higher temperatures above 1000°C [14,15]. Although CrN and CrAlN coatings are frequently used materials and APT analyses on the thermal stability of CrN-containing multilayer coatings [16–19] and CrAlN [20] are available, the effect of measurement parameters on the accuracy of the composition quantification has not been investigated. Thus, within this study, the influence of the laser power on the measured elemental composition of CrN and CrAlN, two materials with different thermal stabilities, was investigated to determine the impact of the thermally-assisted field evaporation on the composition quantification. Therefore, the laser pulse energy was varied systematically, two different laser wavelengths were applied and two different base temperatures were used. For the modification of each parameter, the elemental composition was determined and subsequently compared to the elemental composition obtained by Rutherford backscattering spectrometry (RBS) combined with elastic recoil detection analysis (ERDA).

2. Experimental

The close-to-stoichiometric CrN and CrAlN coatings investigated within this work were synthesized utilizing CemeCon CC800/9 deposition systems. The CrN coating was synthesized on Si (100) substrate with two-fold rotation, using Cr targets from Plansee Composite Materials GmbH at a distance of 7.6 cm between targets and substrate at a temperature of 550°C. The gas pressure was set to 0.58 Pa and a gas mixture of $N_2/(Ar+N_2)$ with a ratio of 0.29 was applied. CrAlN was deposited stationary using a $Cr_{0.4}Al_{0.6}$ target from Plansee Composite Materials GmbH onto a sapphire (0001) substrate with a target-to-substrate distance of 4.5 cm at a temperature of 440°C, the deposition pressure was 0.5 Pa and the $N_2/(Ar+N_2)$ ratio was 0.5. High power pulsed magnetron sputtering was employed using a Melec SIPP2000USB-10-500-S power supply with time-averaged power of 2 kW, pulse on- and off-time of 50 and 1950 µs, respectively, resulting in a peak power density of 0.5 kW cm^{-2}. Accurate chemical compositions were obtained by a combination of RBS and heavy ion ERDA at the Tandem Laboratory of Uppsala University [21] utilizing a 5 MV Pelletron tandem accelerator. Recoils were obtained employing 36 MeV I^{8+} primary ion beam and recorded with a time-of-flight-energy detector telescope. Depth profiles were gained from time-energy coincidence spectra using CONTES [22]. Besides CrN and CrAlN, a stoichiometric TiN reference, previously quantified by RBS/ERDA [23], was measured. The combination of RBS and ERDA exhibits a total uncertainty of the measurement of ± 2.5 %, as recently shown for TiAlN [24]. The films exhibited homogeneous depth profiles and chemical compositions of $Cr_{0.51}N_{0.49}$ and $(Cr_{0.47}Al_{0.53})_{0.49}N_{0.51}$. with oxygen impurities < 0.3 at%.

The APT specimens were prepared using focused ion beam (FIB), via a lift-out process in an FEI Versa 3D and an FEI Helios Nanolab 660 dual-beam microscope following standard procedures for APT specimen preparation as found in refs. [25,26]. The APT measurements were performed using two different CAMECA LEAP systems of type 3000X HR and 4000X HR, equipped with a green ($\lambda = 532$ nm) and an ultraviolet (UV, $\lambda = 355$ nm) laser, respectively. Laser-assisted field evaporation was carried out with constant base temperature as well as pulse frequency in both systems at 60 K and 250 kHz, respectively. Only for one measurement the temperature was decreased to 15 K. The detection rate was set between 5 and 10 ions per 1000 pulses of the laser. The pulse energy of the green laser was varied between 0.1 and 2 nJ, while the pulse energy of the UV laser was increased from 0.01 to 0.18 nJ. In addition, measurements with constant laser pulse energy were performed as well. 10×10^6 ions were acquired for measurements with constant pulse energy, while 5×10^6 ions were collected for each energy segment throughout the laser pulse energy variation.

Reconstruction of the data was done by the software packages IVAS 3.6.14 and IVAS 3.8.0. To minimize the influence of element-dependent thermal tails, ranging of the mass spectra is critical. Thus, the maximum intensity for each peak in the mass spectrum and the onset of the peak from the background were identified, more details on ranging can be found in Ref. [2]. The difference in both mass-to-charge state ratios was used to define a symmetrical range for each peak. Apart from the main elements Cr and N for CrN and Cr, Al and N for CrAlN, also traces of Ga, Ar, O and C with less than 1 at% were detected.

To determine the microstructure and the elemental composition of three exemplary APT specimens after the measurement a transmission electron microscope of type Jeol 2200 FS, equipped with an energy

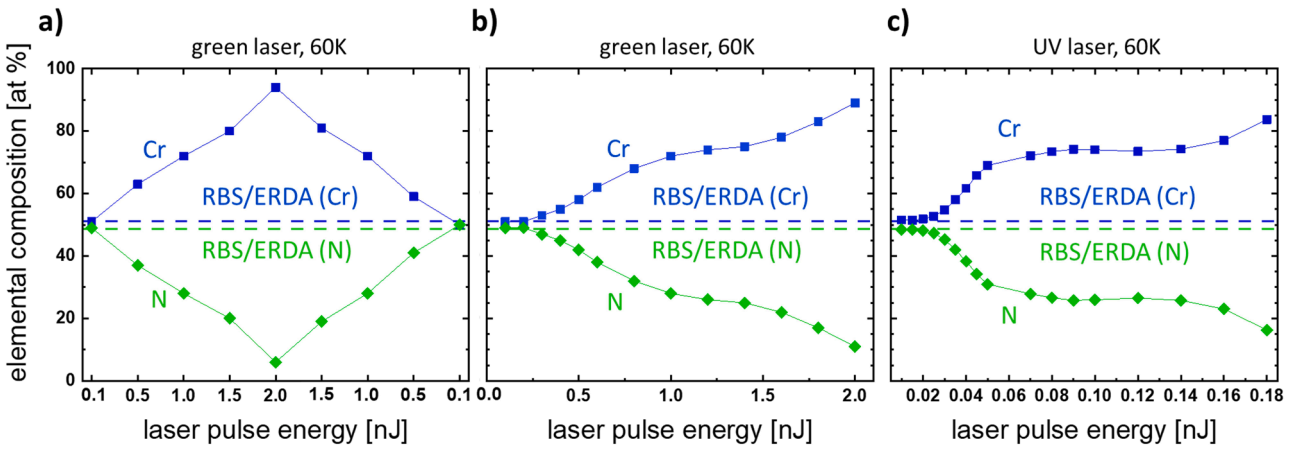

Fig. 2. Evolution of the elemental composition over the laser pulse energy of CrN, measured with a green laser at 60 K with a) a coarse and b) a fine step size and c) measured with a UV laser at 60 K with a fine step size.

dispersive X-ray spectroscopy (EDS) Detector of AZtecTEM X-Max Sensor of Oxford Instruments was used.

3. Results and discussion

Fig. 1a-c show exemplarily the mass spectra for three different laser pulse energies (0.1 nJ, 0.5 nJ and 1.5 nJ, green laser) for different mass-to-charge state ratio ranges. The mass spectra are composed of elemental species (Cr^+, Cr^{2+}, N^+) and molecular ions (N_2^+, CrN^+, CrN^{2+}, Cr_2N^{2+}). Due to the low thermal conductivity of CrN [27,28] pronounced thermal tails are visible. As explained in the experimental section, emphasis was laid on the ranging of the mass spectra to keep the influence of these tails as low as possible. Fig. 1a shows that at 14 Da N^+ is present for the measurements with 0.1 and 0.5 nJ. For the N^+ peak it was recently reported that also some contribution of N_2^{2+} could be present, which would increase the overall N content. The presence of N_2^{2+} may be identified by the occurrence of a characteristic peak at 14.5 Da [2,29]. However, the absence of this peak in Fig. 1a and the reported high electric field of 60 V nm^{-1} necessary for the double ionization of N_2 [30], emphasize that the presence of N_2^{2+} is unlikely. With increasing laser pulse energy, the amount of single charged ions increases. It is visible in Fig. 1b that only very little CrN^{2+} is detected for 1.5 nJ compared to 0.1 and 0.5 nJ, while Cr^+ is only present for 0.5 nJ and 1.5 nJ, as shown in Fig. 1c. This laser pulse energy-dependent ionization can be understood by the decreasing electric field strength with increasing laser pulse energy [9]. Further, the presence of the complex Cr_2N^{2+} (Fig. 1c) can only be observed for the highest laser pulse energy. According to literature, N-carrying molecular ions tend to dissociate during the flight and the neutral fragments cannot be identified by the detector [2,30], which could lead to a falsified measurement of the composition.

A laser pulse energy variation during the measurement of one CrN specimen with 0.1, 0.5, 1, 1.5 and 2 nJ at 60 K using the green laser is shown in Fig. 2a. The laser pulse energy was at first increased from 0.1 up to 2 nJ and subsequently, in a second measurement on a different specimen it was decreased from 2 to 0.1 nJ. The evolution of the Cr and N content over the laser pulse energy is marked by blue squares and green rhombs, respectively. Dashed lines indicate the elemental composition determined by RBS/ERDA, which is close to stoichiometry. For 0.1 nJ the elemental composition obtained by APT is in accordance with RBS/ERDA. With increasing laser pulse energy, the N content strongly decreases to < 10 at% for the highest laser pulse energy of 2 nJ, while a decreasing laser pulse energy leads to the initial close-to-stoichiometric composition. In literature, a decrease of the N content to < 30 at% with increasing laser pulse energy has been observed for other nitrides [2,8,31]. Multiple detection events, molecular ions and preferential evaporation were stated to be possible effects for the N decrease [2,31]. In order to evaluate the evolution of the N content, the laser pulse energy was varied with a finer increment, while keeping all other parameters identical, and the results are shown in Fig. 2b. For the two lowest laser pulse energies (0.1 and 0.2 nJ) a composition close to

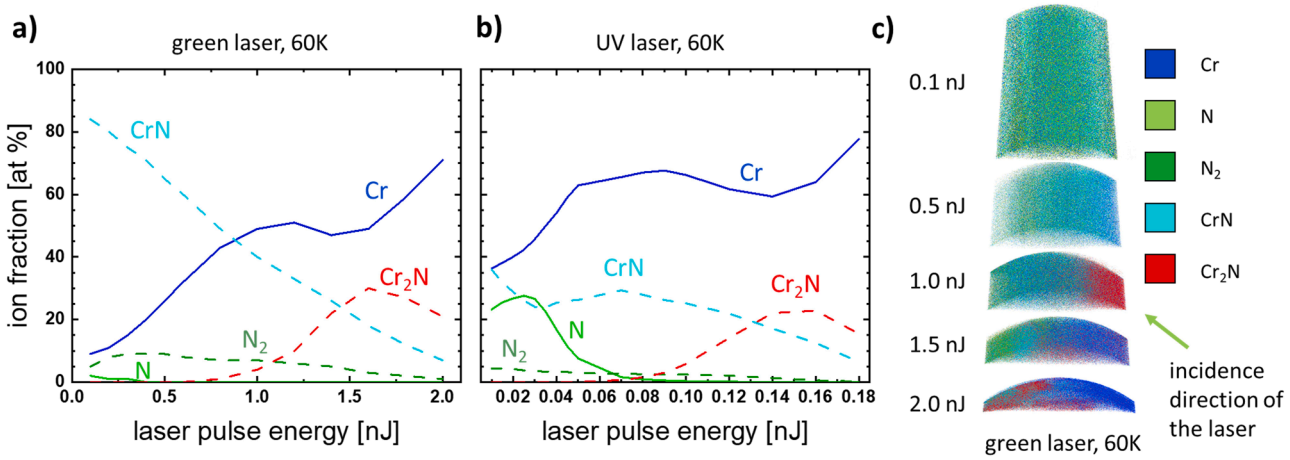

Fig. 3. Evolution of the ion fraction over the laser pulse energy of CrN measured with a) the green laser and b) the UV laser and c) 3D reconstruction of the sectioned specimen, measured with the green laser applying five different laser pulse energies.

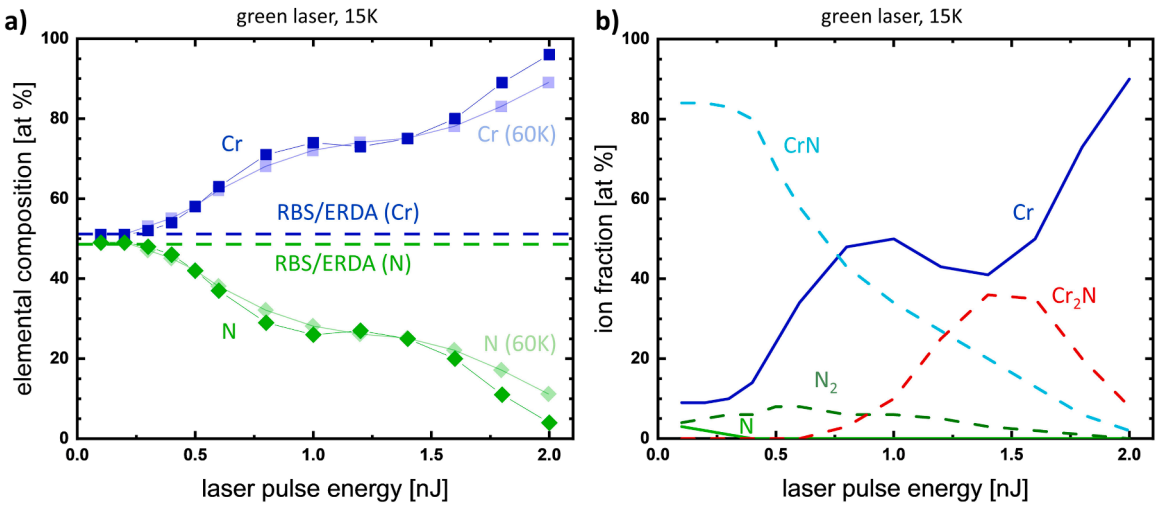

Fig. 4. a) Elemental composition over the laser pulse energy of CrN, measured with the green laser at 15 K compared to the 60 K measurements marked with the faded symbols and b) the corresponding ion fractions to the 15 K measurements.

stoichiometry is obtained. At 0.3 nJ a first decrease of the N content can be seen, which becomes more pronounced up to ~1.0 nJ. Then a slight plateau can be observed, followed again by a more pronounced decrease when increasing the laser pulse energy from 1.6 to 2.0 nJ. The evolution shown in Fig. 2b suggests that two different stages of significant N loss are present. Using the UV laser resulted in the same behavior, see Fig. 2c. This laser is specified to have a smaller spot size and thus, a smaller volume of the specimen is heated up [6]. The laser pulse energy was varied between 0.01 and 0.18 nJ and the diagram exhibits the same trend of the elemental composition as for the measurement with the green laser (Fig. 2b). Thus, it appears that a laser pulse energy of 0.01 to 0.18 nJ for the UV laser is comparable with 0.1 to 2 nJ for the green laser, confirming that the UV laser possesses a higher effective laser energy [6]. The compositional evolution of the UV laser in Fig. 2c reveals that up to a laser pulse energy of ~0.02 nJ, the elemental composition is in good agreement with the composition determined by RBS/ERDA. Starting at ~0.03 nJ a decrease of N is visible. Between 0.07 and 0.14 nJ, the N content is constant, whereas at the highest energies again a N decrease is observed. Thus, for the UV laser also a two-stage N loss is apparent.

Fig. 3a illustrates the detected ion fractions over the laser pulse energy. At the lowest laser pulse energies, the mass spectra are dominated by CrN, which subsequently decreases upon increasing the laser pulse energy. The detected Cr ions first increase, then at laser pulse energies where in Fig. 2b the plateau is observed, they slightly decrease until at even higher energies they increase again. For laser pulse energies $\geq$ 0.8 nJ Cr_2N ions can be detected. The decrease of CrN, the presence of Cr_2N and the strong increase of Cr at the highest laser pulse energies are in good agreement with the decomposition route of CrN [12], indicating a laser-induced thermal decomposition of the specimen during the

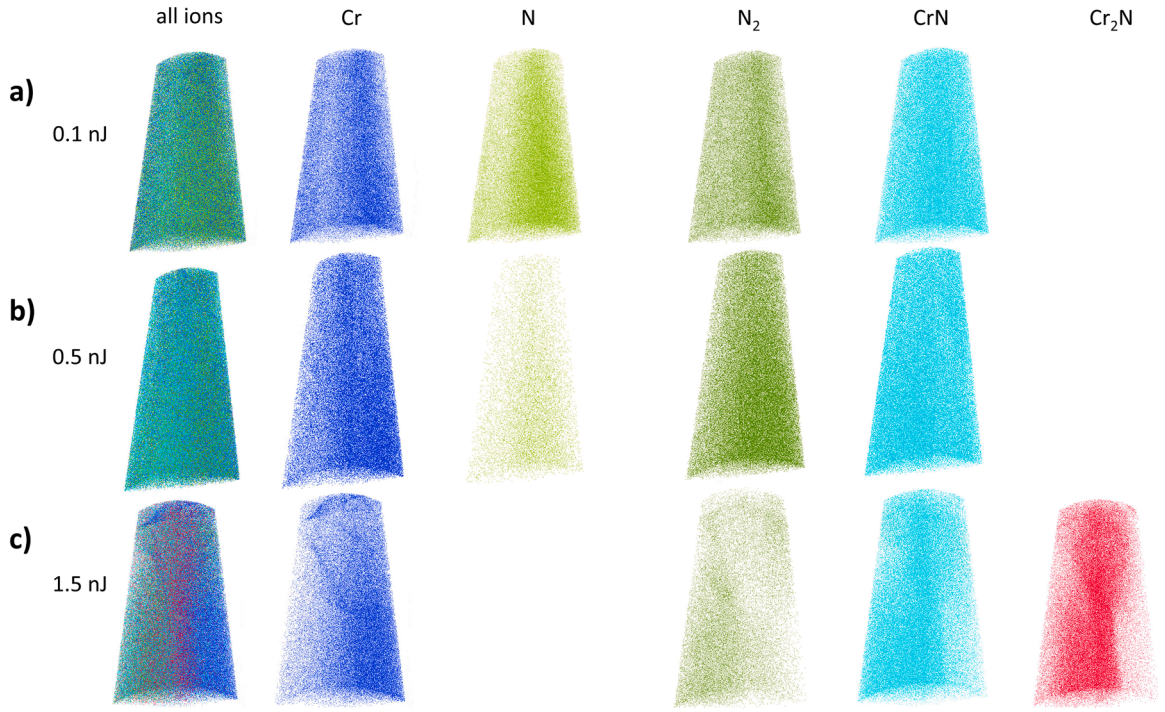

Fig. 5. Reconstruction of three different CrN specimens, measured with a) 0.1 nJ, b) 0.5 nJ and c) 1.5 nJ (green laser) and the visualization of the distribution of the different ion species.

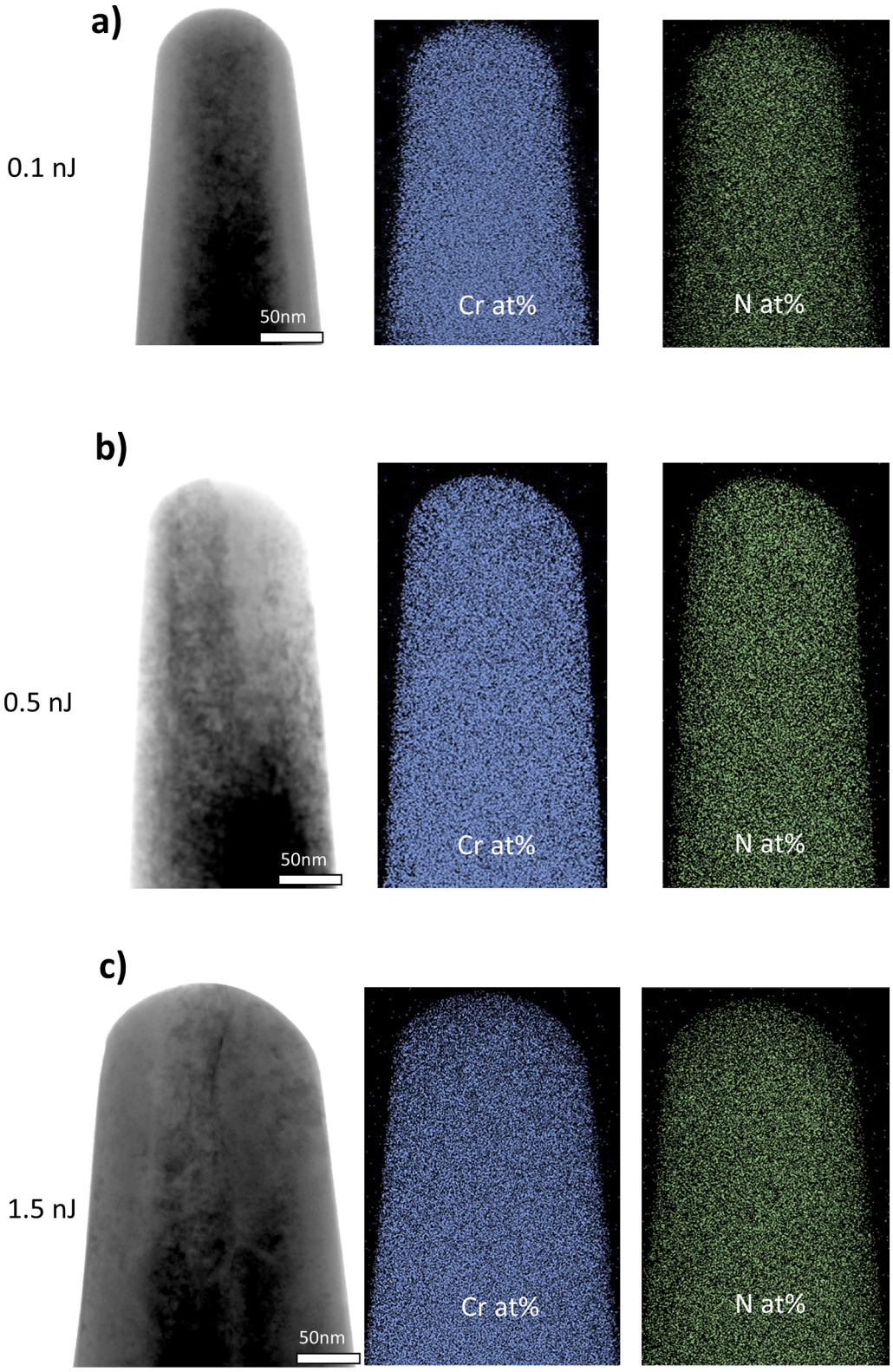

Fig. 6. TEM images with corresponding EDS map for three CrN specimens after the measurement with a) 0.1 nJ, b) 0.5 nJ and c) 1.5 nJ (green laser).

measurement. The evolution of the ion fraction with increasing laser pulse energy for the UV laser, shown in Fig. 3b, is slightly different to the one measured with the green laser (Fig. 3a). The amount of CrN ions at low laser pulse energies is much smaller, while the amount of Cr and N is increased. As the quantification result for low laser pulse energies, e.g. 0.1 nJ (green laser) and 0.01 nJ (UV laser) is very similar (compare Fig. 2b and c), it appears that the UV laser leads to the formation of less molecular ions. Nevertheless, the evolution of the Cr ions and the incidence of Cr_2N in case of the UV laser for pulse energies $\geq$ 0.08 nJ (Fig. 3b) is very similar to the evolution of the ions for the green laser for pulse energies $\geq$ 1 nJ (Fig. 3a). Thus, it can be concluded, that the decomposition stages of CrN during the measurement by laser-assisted

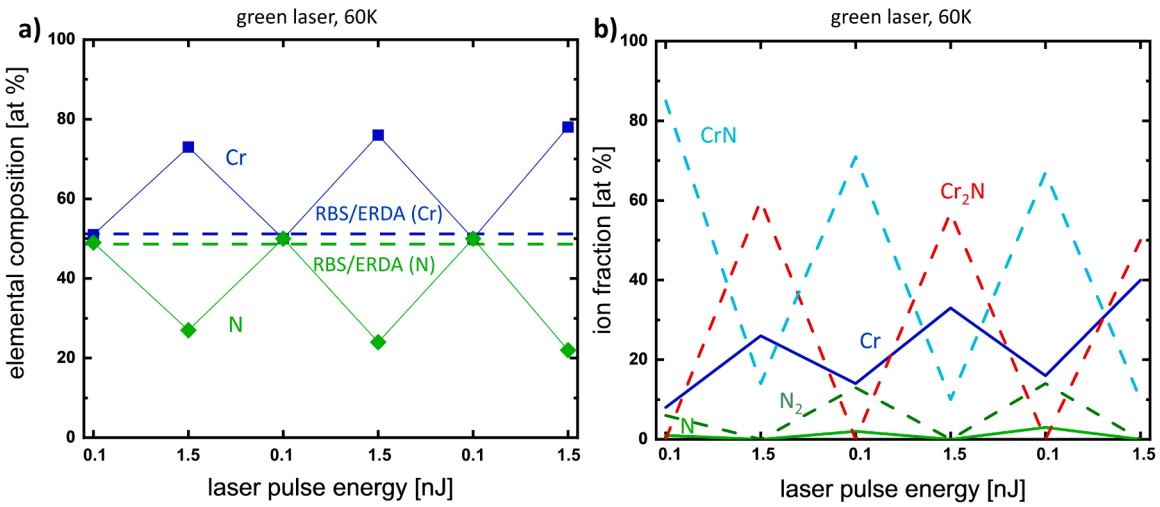

Fig. 7. a) Elemental composition over the laser pulse energy of CrN, measured with the green laser at 60 K, while cycling the laser pulse energy and b) the corresponding ion fractions.

APT occur independently of the employed laser wavelength and spot size. In Fig. 3c the sectioned reconstruction of the specimen with five different energy ranges measured with the green laser is shown. For each section five million ions were collected and thus, the reconstructions become shorter as the cross-section increases. For the lowest laser pulse energy of 0.1 nJ, a homogeneous distribution of the ions can be observed. An increase of the laser pulse energy to 0.5 nJ leads to a segregation of Cr and CrN ions to the right hand side, which coincides with the incidence direction of the laser. At 1 nJ, Cr_2N ions appear instead of CrN on the right hand side of the reconstruction and subsequently transform into Cr ions at 1.5 and 2 nJ, which is also in good agreement with the decomposition route of CrN [12]. It is reasonable to assume that the sequential decomposition of CrN into Cr_2N and Cr is governed by the thermal energy input of the laser. The strong N loss may be explained by the release of gaseous nitrogen, which cannot be ionized by the low electric field at high laser pulse energies [9].

To investigate the influence of the base temperature on the onset of the decomposition, a measurement using the green laser, with increasing pulse energies, was performed at 15 K. Fig. 4a shows the evolution of the Cr and N content over the laser pulse energy for 15 K with the full symbols and the faded ones indicate the evolution of the 60 K measurement which is also shown in Fig. 2b. For 0.1 and 0.2 nJ a composition close to stoichiometry is reached, while again the N loss starts at 0.3 nJ. The plateau between 1.0 and 1.4 nJ is more pronounced than for the measurement at 60 K. At the highest laser pulse energies, the N content decreases to < 5 at% in case of 15 K base temperature and, hence, even lower contents than for 60 K. One possible reason for the even higher measured N loss might be, that at lower temperatures higher electric fields are required for the field evaporation [32]. The evolution of ion fractions as a function of laser pulse energy in Fig. 4b are comparable to the ones in Fig. 3a. Thus, it can be stated that a lower base temperature does not shift the onset of the decomposition.

To gain further knowledge on the notion of the measurement-induced thermal decomposition, three different specimens were measured, each one with a different constant laser pulse energy (green laser). In Fig. 5a-c the reconstructions of the measurements are summarized. For 0.1 nJ (Fig. 5a) a homogeneous distribution of the ions can be observed. A lot of N and N_2 ions are visible, while no Cr_2N is detected. Fig. 5b shows the specimen measured at 0.5 nJ, where already a depletion of N is observable. However, still no Cr_2N is visible. Fig. 5c depicts the specimen measured at 1.5 nJ, where no N ions can be detected. In Fig. 5c it can be seen that three different areas are present in the reconstruction: i) the left hand side, where a lot of CrN is present, ii) the middle, where Cr_2N occurs and iii) the right hand side, where Cr is concentrated. It seems that on the right hand side a complete decomposition occurred, whereas in the middle the intermediate state is

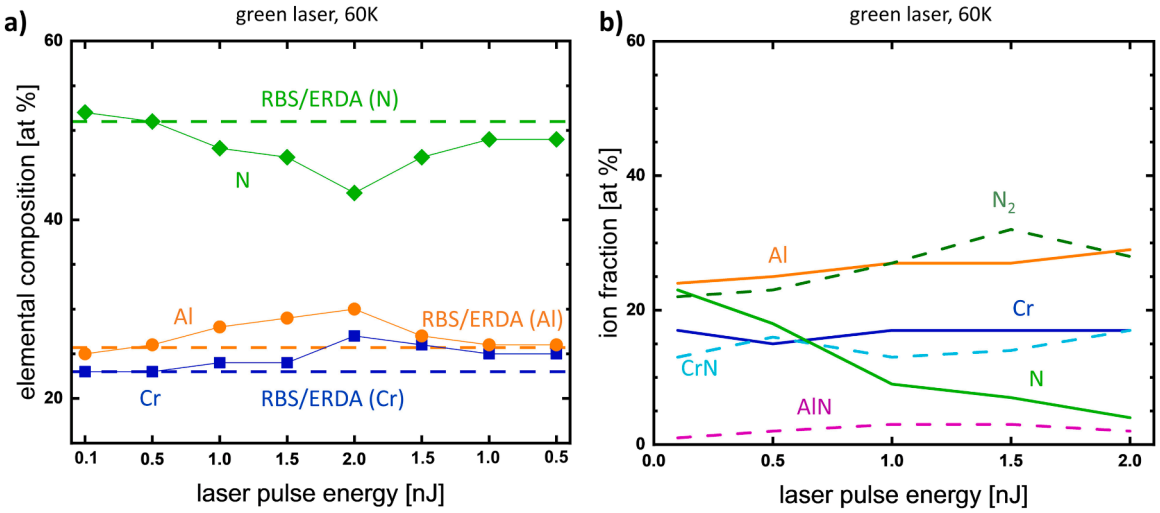

Fig. 8. a) Elemental composition over the laser pulse energy of CrAlN, measured with the green laser at 60 K and b) the corresponding ion fractions.

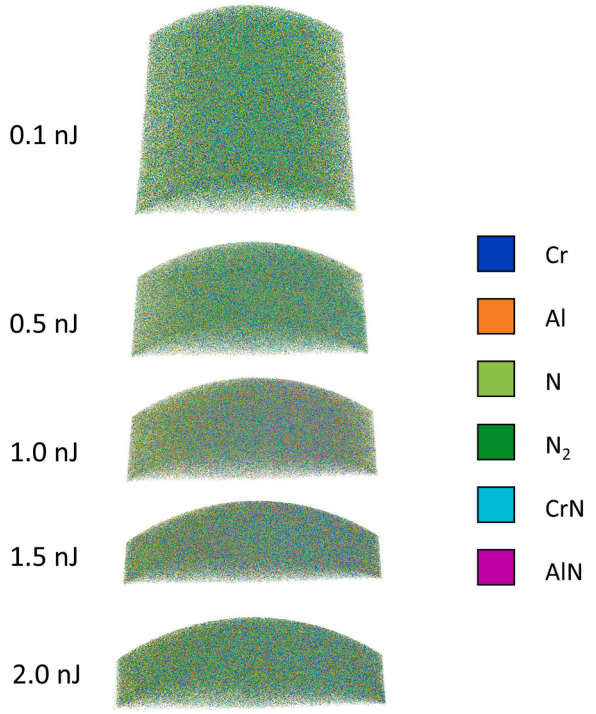

Fig. 9. Sectioned reconstruction of five different laser pulse energy ranges on a CrAlN specimen.

reached and on the left hand side still the CrN is present, which is in accordance with the decomposition route of CrN [12]. The inhomogeneous distribution of the ions can be explained by the incidence direction of the laser on the right hand side, resulting in an inhomogeneity of the evaporation field on the specimen surface. This phenomenon has also been described in literature [33,34].

In a next step the remainder of these three specimens was investigated by TEM, as shown in Fig. 6a-c. It can clearly be seen that all of them exhibit rounding at their top due to the previous measurement. The specimen in Fig. 6c has a larger radius than the other two due to a fracture event during the measurement. The TEM images of all three specimen look quite homogeneous and it seems that the remaining material is not influenced by the laser. In addition, the EDS images reveal a homogeneous distribution of N and Cr over all entire specimens and the elemental composition is close to stoichiometry. Consequently, it can be concluded that the elemental composition of the remaining CrN is not influenced during the measurement. This leads to the suggestion that the decomposition of the CrN just takes place during field evaporation of the uppermost atomic layers. To test this notion a cyclic laser pulse energy variation was performed. Therefore, the laser pulse energy was varied between 0.1 nJ and 1.5 nJ several times. The development of the elemental composition for the different laser pulse energies in Fig. 7a provides evidence that the low laser pulse energy always leads to a composition close to stoichiometry, while 1.5 nJ results for each cycle in a significant N loss. Hence, the measured composition of a cycle at 0.1 nJ is not affected by the previous cycle at 1.5 nJ. The ion fractions over the laser pulse energy in Fig. 7b show that also the detected ions change reversibly. For 0.1 nJ the mass spectrum is dominated by CrN and no Cr_2N ions are detected, whereas at the 1.5 nJ the mass spectrum is dominated by molecular Cr_2N and elemental Cr ions. This reversible change of the elemental composition and the ion fractions supports the notion of CrN decomposition of the uppermost atomic layers.

The measurement of the thermally more stable CrAlN is shown in Fig. 8a. At 60 K with the green laser, the laser pulse energy was increased from 0.1 nJ up to 2 nJ and decreased back down to 0.5 nJ. The composition close to stoichiometry determined by RBS/ERDA is marked with dashed lines. The content of Cr and Al increases with increasing laser pulse energy by 4 and 5 at%, respectively, while the N content decreases from 52 to 43 at%. Fig. 8b depicts the detected ions over the laser pulse energy. Beside the elemental species (Al, Cr and N) also molecular ions (AlN and CrN) can be observed. A higher amount of CrN compared to AlN is present due to the higher binding energy [18]. Further, the detected N ions decrease with increasing laser pulse energy, while N_2 increases. Also, the metallic constituents Cr and Al slightly increase. A similar evolution of composition and ion fractions was observed for experiments with the UV laser (not shown). According to literature the N decrease with increasing laser pulse energy has been explained by multiple detection events, molecular ions and preferential evaporation [2,31]. The evolution of the multiple detection events for the CrAlN measurement series exhibits a decrease of multiplicity with increasing laser pulse energy, which may be attributed to the lower fraction of molecular ions [33]. Thus, the decrease of N is most probably not caused by multiple detection events. As a second explanation, the dissociation of molecular ions was stated [9]. In literature dissociation processes during laser-assisted APT measurements have been demonstrated for different materials [8,30,35]. However, the here presented data cannot be used to prove such dissociation processes, since the LEAP 3000X HR is equipped with a reflectron, that counteracts the energy difference of particles with lower or higher values than estimated [36]. Nevertheless, it seems reasonable that N-containing molecules dissociate during the measurement and that with increasing laser pulse energy less neutral fragments can be ionized, due to the lower electric field strength [9].

In Fig. 9 the reconstruction of a CrAlN specimen, measured with five different laser pulse energies, is shown. The distribution of the ions is homogeneous over the whole measurement and no separation as in case of CrN (compare Fig. 3c and Fig. 5c) is visible. The minor N decrease and the homogeneous ion distribution for CrAlN compared to CrN lead to the assumption that no decomposition of the CrAlN upon increasing the laser pulse energy occurs which can be rationalized by the higher thermal stability of CrAlN.

4. Conclusions

Within this study we investigated the influence of the laser pulse parameters on the elemental composition by performing laser-assisted atom probe tomography (APT) on CrN and CrAlN in comparison to accurate ion beam analysis data. It was shown that an increasing laser pulse energy has a major impact on the elemental composition. Especially for CrN a strong decrease of the N content could be determined and the detected ions indicated decomposition of CrN following the typically observed decomposition route into Cr_2N and subsequently into Cr and gaseous N upon increasing the laser pulse energy. Considering the reconstruction of the specimen measured with increasing laser pulse energy an inhomogeneous distribution of the ions was observed. The thermally induced decomposition started at the incidence area of the laser. TEM investigations of the residue of measured specimens in combination with cyclic APT measurements revealed that the decomposition only occurs within the uppermost atomic layers and that the elemental composition of the rest of the material is not influenced. Further, it could be shown that the base temperature and the laser wavelength as well as the laser spot size do not affect the evolution of the measured elemental composition. The CrAlN showed no decomposition during the measurement, which can be rationalized by its higher thermal stability. The lower decrease of the N content for CrAlN, obtained with increasing laser pulse energy could be explained by the dissociation of molecular ions occurring at higher energies. The present study highlights the importance to determine suitable parameters for APT measurements to ensure the detection of the accurate elemental composition.

Declaration of Competing Interest

The authors declare that they have no known competing financial interests or personal relationships that could have appeared to influence the work reported in this paper.

Data Availability

Data will be made available on request.

Acknowledgments

The financial support by the Austrian Federal Ministry for Digital and Economic Affairs and the National Foundation for Research, Technology and Development is gratefully acknowledged. This research was also funded by German Research Foundation (DFG, SFB-TR 87/3) "Pulsed high power plasmas for the synthesis of nanostructured functional layers". Transnational access to the ion beam analysis facility at Uppsala University has been supported by the RADIATE project under the Grant Agreement 824096 from the EU Research and Innovation program HORIZON 2020. Accelerator operation at Uppsala University has been supported by the Swedish research council VR-RFI (#2019-00191). The authors gratefully acknowledge the financial support of the European Research Council (ERC) under the European Union's Horizon 2020 research and innovation program (Grant No. 771146 TOUGHIT).

References

[1] M. Tkadletz, N. Schalk, R. Daniel, J. Keckes, C. Czettl, C. Mitterer, Advanced characterization methods for wear resistant hard coatings: a review on recent progress, Surf. Coatings Technol. 285 (2016) 31–46, https://doi.org/10.1016/J.SURFCOAT.2015.11.016.
[2] M. Hans, J.M. Schneider, On the chemical composition of TiAlN thin films - Comparison of ion beam analysis and laser-assisted atom probe tomography with varying laser pulse energy, Thin Solid Films 688 (2019), 137251, https://doi.org/10.1016/j.tsf.2019.04.026.
[3] M.K. Miller, T.F. Kelly, K. Rajan, S.P. Ringer, The future of atom probe tomography, Mater. Today. 15 (2012) 158–165, https://doi.org/10.1016/S1369-7021(12)70069-X.
[4] T.F. Kelly, M.K. Miller, Invited review article: Atom probe tomography, Rev. Sci. Instrum. (2007) 78, https://doi.org/10.1063/1.2709758.
[5] G.L. Kellogg, T.T. Tsong, Pulsed-laser atom-probe field-ion microscopy, J. Appl. Phys. 51 (1980) 1184–1193, https://doi.org/10.1063/1.327686.
[6] D. Santhanagopalan, D.K. Schreiber, D.E. Perea, R.L. Martens, Y. Janssen, P. Khalifah, Y.S. Meng, Effects of laser energy and wavelength on the analysis of $LiFePO_4$ using laser assisted atom probe tomography, Ultramicroscopy 148 (2015) 57–66, https://doi.org/10.1016/j.ultramic.2014.09.004.
[7] E. Di Russo, I. Blum, J. Houard, G. Da Costa, D. Blavette, L. Rigutti, Field-dependent measurement of GaAs composition by atom probe tomography, Microsc. Microanal. 23 (2017) 1067–1075, https://doi.org/10.1017/S1431927617012582.
[8] E. Di Russo, I. Blum, J. Houard, M. Gilbert, G. Da Costa, D. Blavette, L. Rigutti, Compositional accuracy of atom probe tomography measurements in GaN: Impact of experimental parameters and multiple evaporation events, Ultramicroscopy 187 (2018) 126–134, https://doi.org/10.1016/j.ultramic.2018.02.001.
[9] M. Hans, J.M. Schneider, Electric field strength-dependent accuracy of TiAlN thin film composition measurements by laser-assisted atom probe tomography, New J. Phys. 22 (2020) 1–9, https://doi.org/10.1088/1367-2630/ab7770.
[10] C. Mitterer, PVD and CVD Hard coatings. Compr. Hard Mater., Elsevier Ltd, Amsterdam, 2014, pp. 449–467, https://doi.org/10.1016/B978-0-08-096527-7.00035-0.
[11] J. Almer, M. Odén, L. Hultman, G. Håkansson, Microstructural evolution during tempering of arc-evaporated Cr–N coatings, J. Vac. Sci. Technol. A Vacuum, Surfaces, Film. 18 (2000) 121–130, https://doi.org/10.1116/1.582128.
[12] W. Ernst, J. Neidhardt, H. Willmann, B. Sartory, P.H. Mayrhofer, C. Mitterer, Thermal decomposition routes of CrN hard coatings synthesized by reactive arc evaporation and magnetron sputtering, Thin Solid Films 517 (2008) 568–574, https://doi.org/10.1016/j.tsf.2008.06.086.
[13] P.H. Mayrhofer, F. Rovere, M. Moser, C. Strondl, R. Tietema, Thermally induced transitions of CrN thin films, Scr. Mater. 57 (2007) 249–252, https://doi.org/10.1016/j.scriptamat.2007.03.058.
[14] H. Willmann, P.H. Mayrhofer, P.O.. Persson, A.E. Reiter, L. Hultman, C. Mitterer, Thermal stability of Al-Cr-N hard coatings, Scr. Mater. 54 (2006) 1847–1851, https://doi.org/10.1016/j.scriptamat.2006.02.023.
[15] P.H. Mayrhofer, H. Willmann, A.E. Reiter, Structure and phase evolution of Cr-Al-N coatings during annealing, Surf. Coatings Technol. 202 (2008) 4935–4938, https://doi.org/10.1016/j.surfcoat.2008.04.075.
[16] D. Tytko, P.P. Choi, D. Raabe, Oxidation behavior of AlN/CrN multilayered hard coatings, Nano Converg. 4 (2017) 2–6, https://doi.org/10.1186/s40580-017-0109-y.
[17] I. Povstugar, P.P. Choi, D. Tytko, J.P. Ahn, D. Raabe, Interface-directed spinodal decomposition in TiAlN/CrN multilayer hard coatings studied by atom probe tomography, Acta Mater. 61 (2013) 7534–7542, https://doi.org/10.1016/j.actamat.2013.08.028.
[18] P.P. Choi, I. Povstugar, J.P. Ahn, A. Kostka, D. Raabe, Thermal stability of TiAlN/CrN multilayer coatings studied by atom probe tomography, Ultramicroscopy 111 (2011) 518–523, https://doi.org/10.1016/j.ultramic.2010.11.012.
[19] D. Tytko, P.P. Choi, D. Raabe, Thermal dissolution mechanisms of AlN/CrN hard coating superlattices studied by atom probe tomography and transmission electron microscopy, Acta Mater. 85 (2015) 32–41, https://doi.org/10.1016/j.actamat.2014.11.004.
[20] M. Meindlhumer, T. Ziegelwanger, J. Zalesak, M. Hans, L. Löfler, S. Spor, N. Jäger, A. Stark, H. Hruby, R. Daniel, D. Holec, J.M. Schneider, C. Mitterer, J. Keckes, Precipitation-based grain boundary design alters Inter- to Trans-granular Fracture in AlCrN Thin Films, Acta Mater. 237 (2022), 118156, https://doi.org/10.1016/j.actamat.2022.118156.
[21] P. Ström, D. Primetzhofer, Ion beam tools for nondestructive in-situ and in-operando composition analysis and modification of materials at the Tandem Laboratory in Uppsala, J. Instrum. (2022) 17, https://doi.org/10.1088/1748-0221/17/04/P04011.
[22] M. Janson, CONTES Instruction Manual, Internal Report, Uppsala University, Sweden, 2004.
[23] M.A. Sortica, V. Paneta, B. Bruckner, S. Lohmann, M. Hans, T. Nyberg, P. Bauer, D. Primetzhofer, Electronic energy-loss mechanisms for H, He, and Ne in TiN, Phys. Rev. A. 96 (2017) 1–7, https://doi.org/10.1103/PhysRevA.96.032703.
[24] M. to Baben, M. Hans, D. Primetzhofer, S. Evertz, H. Ruess, J.M. Schneider, Unprecedented thermal stability of inherently metastable titanium aluminum nitride by point defect engineering, Mater. Res. Lett. 5 (2017) 158–169, https://doi.org/10.1080/21663831.2016.1233914.
[25] M.K. Miller, K.F. Russell, G.B. Thompson, Strategies for fabricating atom probe specimens with a dual beam FIB, Ultramicroscopy 102 (2005) 287–298, https://doi.org/10.1016/j.ultramic.2004.10.011.
[26] K. Thompson, D. Lawrence, D.J. Larson, J.D. Olson, T.F. Kelly, B. Gorman, In situ site-specific specimen preparation for atom probe tomography, Ultramicroscopy 107 (2007) 131–139, https://doi.org/10.1016/j.ultramic.2006.06.008.
[27] W. Martienssen, H. Warlimont (Eds.), Condensed matter and materials data, eds., Spinger Berlin Heidelberg New York, 2011 https://doi.org/10.1007/s13398-014-0173-7.2.
[28] M.K. Samani, G.C.K. Chen, X.Z. Ding, X.T. Zeng, Thermal conductivity of CrAlN and TiAlN coatings deposited by lateral rotating cathode arc, Key Eng. Mater. 447 448 (2010) 705–709, https://doi.org/10.4028/www.scientific.net/KEM.447-448.705.
[29] I. Citlalli, S. Benítez, Defect-engineered (Ti, Al) N thin films, 2017.
[30] B. Gault, D.W. Saxey, M.W. Ashton, S.B. Sinnott, A.N. Chiaramonti, M.P. Moody, D. K. Schreiber, Behavior of molecules and molecular ions near a field emitter, New J. Phys. 18 (2016), https://doi.org/10.1088/1367-2630/18/3/033031.
[31] L. Mancini, N. Amirifar, D. Shinde, I. Blum, M. Gilbert, A. Vella, F. Vurpillot, W. Lefebvre, R. Lardé, E. Talbot, P. Pareige, X. Portier, A. Ziani, C. Davesnne, C. Durand, J. Eymery, R. Butté, J.F. Carlin, N. Grandjean, L. Rigutti, Composition of wide bandgap semiconductor materials and nanostructures measured by atom probe tomography and its dependence on the surface electric field, J. Phys. Chem. C. 118 (2014) 24136–24151, https://doi.org/10.1021/jp5071264.
[32] G.L. Kellogg, Temperature dependence of the silicon field evaporation voltage, Surf. Sci. 124 (1983) 55–59.
[33] R. Kirchhofer, M.C. Teague, B.P. Gorman, Thermal effects on mass and spatial resolution during laser pulse atom probe tomography of cerium oxide, J. Nucl. Mater. 436 (2013) 23–28, https://doi.org/10.1016/j.jnucmat.2012.12.052.
[34] Y.H. Chang, I. Mouton, L. Stephenson, M. Ashton, G.K. Zhang, A. Szczpaniak, W. J. Lu, D. Ponge, D. Raabe, B. Gault, Quantification of solute deuterium in titanium deuteride by atom probe tomography with both laser pulsing and high-voltage pulsing: Influence of the surface electric field, New J. Phys. 21 (2019), https://doi.org/10.1088/1367-2630/ab1c3b.
[35] D. Zanuttini, I. Blum, L. Rigutti, F. Vurpillot, J. Douady, E. Jacquet, P.M. Anglade, B. Gervais, Simulation of field-induced molecular dissociation in atom-probe tomography: Identification of a neutral emission channel, Phys. Rev. A. 95 (2017) 1–6, https://doi.org/10.1103/PhysRevA.95.061401.
[36] D.W. Saxey, Correlated ion analysis and the interpretation of atom probe mass spectra, Ultramicroscopy 111 (2011) 473–479, https://doi.org/10.1016/j.ultramic.2010.11.021.